Surface gravity waves and their acoustic signatures, 1 - 30 Hz, on the mid-Pacific sea floor.

W. E. Farrell[1] and Walter Munk[2]
[1] 13765 Durango Drive, Del Mar CA 92014
[2] University of California San Diego SIO-IGPP, 9500 Gilman Drive Mail Code 0225, La Jolla CA 92093-0225

(Dated: August 26, 2012)

In 1999 Duennebier *et al.* deployed a hydrophone and geophone below the conjugate depth in the abyssal Pacific, midway between Hawaii and California. Real time data were transmitted for three years over an abandoned ATT cable. These data have been analyzed in the frequency band 1 to 30 Hz. Between 1 and 6 Hz the bottom data are interpreted as acoustic radiation from surface gravity waves, an extension to higher frequencies of a non-linear mechanism proposed by Longuet-Higgins in 1950 to explain microseisms. The inferred surface wave spectrum for wave lengths between 6 m and 17 cm is saturated (wind-independent) and roughly consistent with the traditional Phillips κ^{-4} wave number spectrum. Shorter ocean waves have a strong wind dependence and a less steep wave number dependence. Similar features are found in the bottom record between 6 and 30 Hz. But this leads to an enigma: the derived surface spectrum inferred from the Longuet-Higgins mechanism with conventional assumptions for the dispersion relation is associated with mean square slopes that greatly exceed those derived from glitter. Regardless of the generation mechanism, the measured bottom intensities between 10 and 30 Hz are well below minimum noise standards reported in the literature.

PACS numbers: 43.30.Nb (Noise in water), 43.28.Py (Interaction of fluid motion and sound)

I. INTRODUCTION

More than fifty years ago, Longuet-Higgins, then Hasselmann, explained the generation of microseisms on the deep sea floor by a nonlinear process associated with surface gravity waves. The linear wave amplitude diminishes by a factor $\exp(-2\pi)$ per wavelength and is thus totally negligible at depth, but under some circumstances a slight fraction of the wave energy is converted into acoustic radiation at twice the wave frequency (but of much greater length) which reaches the sea bottom. The Longuet-Higgins and Hasselmann theory was generalized by Brekhovskikh and others to allow for surface tension. There are inconsistencies and errors, and we have found it necessary to summarize the theory in an Appendix.

The theory calls for oppositely traveling surface waves (almost opposite in the Hasselmann treatment) so that twice during each wave period all the energy is potential and twice kinetic (hence the double frequency). The original application was to an ocean swell reflected by a steep continental slope and to long ocean waves from two opposing storm fetches. Here we attempt to interpret H2O[1] hydrophone and geophone records on the deep sea floor in the frequency band 1 - 30 Hz in terms of the same nonlinear process, a bold extension to centimeter and even millimeter scale. We are encouraged by the smooth blending with numerical wave models at the low end of the band, and by rough agreement with the Phillips spectrum in the middle. There are inconsistencies, however, above 6 Hz, in the ultragravities. Others have suggested bubbles associated with breaking waves as generators of deep ocean noise in this frequency range.

There have been numerous papers analyzing H2O data in the decade since the station ceased operation. None, however, has focused on our band of study. The recent paper by Duennebier *et al*[2] applies an approach similar to ours (see Discussion) to develop wave models consistent with deep sea data from the ALOHA station, some 100 km N. of Ohau. The Duennebier paper is also to be recommended for the citations to other analyses of H2O data in its exhaustive bibliography.

II. ACOUSTIC RADIATION FROM SURFACE WAVES

The following interpretation of bottom spectra is founded on one premise and two models. The premise is that the ambient fluctuations on the bottom are attributable to acoustic radiation from interfering wind waves on the surface. Two models are required, a wave model and an acoustic model. The following description of the models recapitulates our previous work with minor extensions.[3,4]

The model for the azimuthally averaged, or 1-d, wave elevation spectrum, $F_\zeta(\kappa, U)$, using radian wave number with U wind speed, is the combination of two components: (i) a saturated (independent of wind speed) Phillips-like gravity wave spectrum, and (ii) a wind-dependent ultragravity spectrum:

$$F_\zeta(\kappa, U) = \frac{1}{2}\beta\kappa^m + \gamma\exp(aU)\kappa^n \qquad (1)$$

Each component is given a simple power-law dependence on wave number. The five parameters of the model are adjusted so it fits the H2O data, as described below. Using H for the spreading function, the 2-d spectrum, in polar coordinates, is

$$F_\zeta(\kappa, U, \theta) = F_\zeta(\kappa, U)H_\kappa(U, \theta), \qquad (2a)$$

$$\int_{-\pi}^{\pi} H_\kappa(U, \theta)d\theta = 1 \qquad (2b)$$

with mean square elevation and slope

$$\langle \zeta^2 \rangle = \int_0^\infty F_\zeta(\kappa, U)\kappa d\kappa, \tag{3a}$$

$$\langle m^2 \rangle = \int_0^\infty \kappa^2 F_\zeta(\kappa, U)\kappa d\kappa, \tag{3b}$$

respectively

The relation between the deep pressure spectrum (with radian acoustic frequency ω_A) and the surface elevation spectrum (frequency $\omega_S = \omega_A/2$, and wave number κ_S) is written (see A.11)

$$F_p(\omega_A) = \left[\frac{\pi}{8}\left(\frac{\rho}{c}\right)^2 \omega_A^6 \frac{\kappa_S}{v}\right] F_\zeta^2(\kappa_S)\, R_B^2\, I_\kappa\, B \tag{4}$$

where $v = v(\kappa_S)$ is the group velocity of the surface waves and $B = B(\omega_A, \theta, \lambda)$ is appended to account for the influence of the ocean's variable sound speed and bottom.

Sea water density and sound speed are ρ, c. The factors R_B, I_κ, and B are all taken as constants, with $R_B = 1$ (ignoring the Brekhovskikh ratio), $I_\kappa = (2\pi)^{-1}$ (assuming directional isotropy), and $B = 1$ (ignoring the sound speed profile and bottom interaction).

Bottom velocity data are as informative as pressure. For waves in an acoustic medium, the pressure and velocity component in the direction of propagation are related by the impedance $Z = \rho c$. Analogously, we define effective impedances Z_{ev}, Z_{eh} relating vertical and horizontal components of velocity to pressure. In terms of the spectra,

$$F_v(\omega) = Z_{ev}^{-2} F_p(\omega), \quad F_h(\omega) = Z_{eh}^{-2} F_p(\omega), \tag{5a}$$

$$Z = Z(\omega, \theta, \lambda) \tag{5b}$$

In the case of a bottomless, constant velocity ocean, with the source a homogeneous surface layer of incoherent dipoles, $B = 1$ and the effective impedances are given by

$$Z_{ev}^2 = 2(\rho c)^2 = 126.5\,\text{dB},\ Z_{eh}^2 = 4(\rho c)^2 = 129.5\,\text{dB} \tag{6}$$

III. EVIDENCE FROM BENEATH THE SEA SURFACE

Fig. 1 shows spectra selected from 3 years of H2O recordings on the deep sea floor. Spectra were calculated for 3 hour windows to a resolution of 0.1 Hz, giving about 2000 equivalent degrees of freedom. The velocity spectra (geophone sensor, channels EHZ, EH1, EH2) are superior in quality; the pressure spectra (hydrophone sensor, channel HDH) are consistent with the independently recorded velocities, but are obstructed by noise at the higher frequencies. The smooth curves are model spectra fitted to the pressure and velocity fields, using visual judgement, based on the theory described above (equations 1, 4, and 5a), with

$$m = -4.25, \quad \beta = 0.01, \tag{7a}$$

$$n = -2.15, \quad \gamma = 1.06 \times 10^{-7}, \quad a = .31, \text{ and} \tag{7b}$$

$$Z_{ev}^2 = 117\text{ dB} \tag{7c}$$

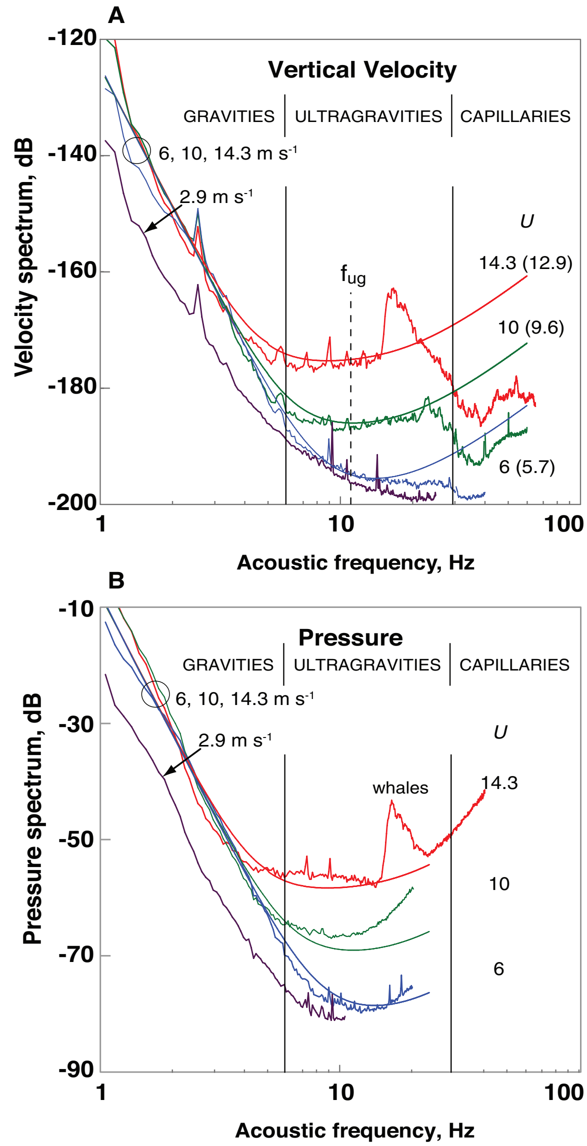

FIG. 1. Bottom spectra at H2O modeled as acoustic radiation from interfering wind waves on the ocean surface. The three pairs of spectra, data and model, are labeled with two wind speeds in the upper panel. The first is inferred from the data itself and the parenthetical is the ECMWF wind at the time. The two strongest spectra are for 3 hr time windows taken in year 2000, days 33.8, 284.1; the blue and purple are for days 148.3 and 157.6 in 2001. These exemplars are representative of tens to hundreds of virtually identical spectra at the respective wind speeds. SI units are used throughout, Pa^2/Hz for pressure and $(\text{m}\,\text{s}^{-1})^2/\text{Hz}$ for velocity.

In assessing the wind dependence we have used wind speeds at 6-hourly intervals provided by the European Center for Medium-Range Weather Forecasts (ECMWF). Data from ERA-Interim, the latest ECMWF global atmospheric reanalysis of the period 1979 to present, were interpolated from the analysis grid to provide values over the H2O location. These, in turn, were interpolated with respect to time to the analysis windows.

A. Gravities

With regard to the gravity waves, there is rough agreement between the derived model and ocean wave observations. The "Phillips constant," $\beta = 0.01$, compares to the Pierson and Moskowitz value of 0.0081,[5,6] and the shape of the wave number spectrum, $F_\zeta(\kappa) \propto \kappa^{-4.25}$, compares to the classical $F_\zeta(\kappa) \propto \kappa^{-4}$.

In the frequency domain, ocean waves with a κ^{-4} wave number spectrum yield an ω^{-5} frequency spectrum by (A.9) and (A.2). For the acoustic radiation from such waves, $F_p(\omega) \propto \kappa^{-7}$ by (A.5). Our ocean wave model for the gravities leads to $F_\zeta(\omega) \propto \omega^{-5.5}$ and $F_p(\omega) \propto \omega^{-8}$.

Bottom and surface spectra are both saturated for moderate and strong winds. At very weak winds the spectrum (purple) falls beneath saturation. In a previous paper[4] we have attributed this to a decrease in the overlap integral. In this special case, the pressure record is better: the velocity spectrum for light winds and $f \gtrsim 4$ Hz is limited by sensor noise.

B. Ultragravities

The band $6 < f_A < 30$ Hz is labeled "ultragravities," in analogy with the short ultragravity waves on the ocean's surface. These spectra clearly are not saturated. The acoustic transitions from the steep spectrum to the flat spectrum, occurring between 4 and 10 Hz, are consistent with the measured transitions in the surface wave field. An interesting feature is the drop by about 10 dB for moderate and high winds (ignoring whale noise) at about 30 Hz. This second transition is close to twice 13.5 Hz, the boundary between ultragravity and capillary waves. This is the frequency of the minimum phase velocity and, perhaps more importantly, where the phase and group velocities are equal.

The wave number exponent of the ultragravities, $n = -2.15$, sets the curvature of the acoustic model, and the constant γ sets the level. These were selected by visually matching the model spectra to numerous observed spectra. The acoustic floor at reference frequency $f_{ug} = 11.5$ is near -197 dB (re $(\mathrm{m\,s^{-1}})^2$/Hz) and -80 dB (re Pa^2/Hz) for the geophone and hydrophone. This probably is set by instrument noise, but we cannot dismiss the possibility it represents the integrated effect of acoustic radiation from distant wave motion.

A sorting of nearly 2000 H2O velocity-wind pairs at f_{ug} suggests exponential dependence on wind speed with an increase by $2.7\,\mathrm{dB}/(\mathrm{m\,s^{-1}})$ (Fig. 2). At 22 Hz (not shown) the acoustic floor is -199 dB and the rise slightly steeper. The combined analysis suggests a $2.9\,\mathrm{dB}/(\mathrm{m\,s^{-1}})$ dependence of the ultragravity spectrum.

Data for low winds are not helpful because of the acoustic floor, and high winds at this latitude are scarce, so the usable range of wind speeds for parameterizing the dependence of the ultragravity spectrum on U is limited. For example, if the wind dependence is modeled as a power law, the histogram shown in Fig. 2 is reasonably fit by the function $F_v = -246.9 + 60\log(U)$. The difference between this function and the exponential, for $5.5 < U < 14\ \mathrm{m\,s^{-1}}$ is no more than $1\ \mathrm{m\,s^{-1}}$. Using the power law, an alternative expression for the ultragravity term in (1) is $2.46 \times 10^{-9} U^3 \kappa^{-2.15}$.

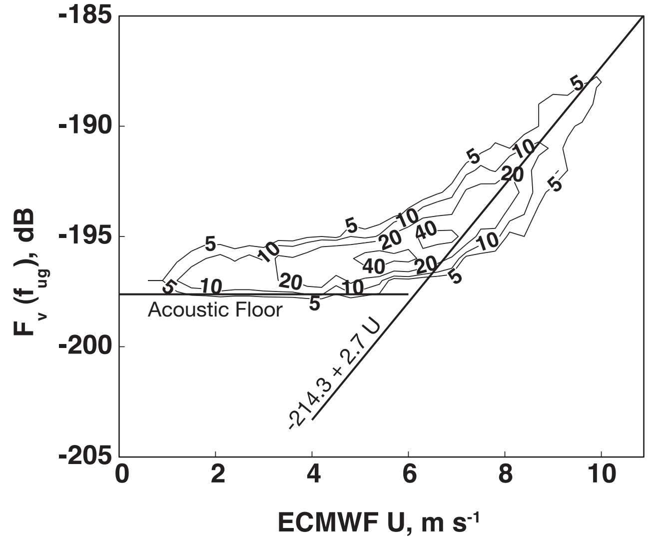

FIG. 2. The variation with wind of the geophone spectral intensity at $f_{ug} = 11.5$ Hz (see Fig. 1) can be modeled as an exponential for speeds greater than about $6.5\ \mathrm{m\,s^{-1}}$. In this two dimensional histogram, the contours refer to the number of spectra (out of 1787 total) within 1 dB $\times$ $0.3\ \mathrm{m\,s^{-1}}$ cells.

The ultragravities are commonly taken to have a power law dependence on wind speed U, or equivalently friction velocity $u_\star$ ($U \approx 25u_\star$). For example, in an analysis of microwave scattering across multiple radio bands, Hwang[7] fit the data to a function of the form $F_\zeta \propto u_\star^\alpha$. He found $0.5 < \alpha < 2$, as the wave number ranges from the low end of the ultragravities band to the gravity/capillary transition.

The ultragravity acoustic spectrum in the band 6 to 30 Hz is a reliable proxy for surface winds. But the good agreement may in part be circular. Wind models uniformly distributed in space and time are obtained by assimilating the patchy satellite estimates into numerical weather models. Satellite winds are in part based on empirical relations involving the scattering cross-sections of waves in the ultragravity band.

C. Sensitivity of bottom receivers to surface processes

For a temperate sound channel in an ocean of 5 km depth, the *direct* field of view is limited to an overhead circle of 32 km radius centered above the bottom recorders (Fig. 3). At that distance rays with 13 degrees surface inclination are tangent to the sea floor. Flatter rays from sources outside the circle turn above the bottom: the sea floor is in the geometric ray shadow. The intensity of the received bottom signal depends upon the directivities of the emitted surface radiation and the recorded bottom radiation. In addition to this direct radiation, acoustic energy will reach the bottom recorders in the form of trapped seismic waves from remote regions.[8,9]

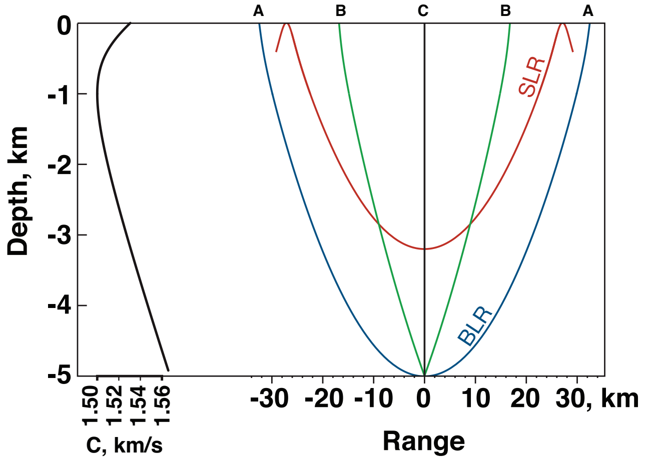

FIG. 3. Rays in the temperate sound channel, left.[10] The surface limited ray (SLR), with inclination of 12° at the sound axis, turns at the "surface conjugate" depth of 3.2 km; beneath this depth, noise sources (such as whales) cannot be heard except by surface reflection. The ocean beneath 3.2 km is in the "shadow zone." The bottom limited ray (BLR), with axial inclination of 17°, intersects the surface around a circle with a radius of 32 km. Sound waves from dipole sources associated with surface waves within the 32 km circle (at A, B, C) are received by bottom hydrophones along three direct paths, as shown; seismic waves from remote scattering also reach the bottom hydrophones.

For the case of a homogeneous layer of incoherent dipole sources on the surface of a uniform ocean, 90 % of the pressure energy arises from within a circle of diameter 6 times the receiver depth, or 30 km for the 5 km receiver (Ref. 3, Eqn. 7). This is somewhat less than the zone BB in Fig. 3. For the vector receiver, the 90% range is a little less for the vertical component and a little more for the horizontal. Thus, the refraction of rays by the sound channel is a second order effect for deep receivers.

D. Junction with long gravity waves

The H2O-derived wave model (Eq. 1, 7) blends smoothly with ECMWF models[11] at 0.5 Hz (Fig. 4); both models are saturated for strong winds and slightly below saturation for $U \leq 5\,\mathrm{m\,s^{-1}}$. Yet they are derived from very different approaches: H2O from bottom observations 5 km beneath the surface, ECMWF from space observations 500 km above the sea surface assimilated into wind-wave weather models.

Either model can easily be extended into the other's domain, for H2O by extending the spectra to lower frequencies and for ECMWF by extending the energy balance to higher frequencies. But the many underlying assumptions suggest that we regard the smooth junction with caution.

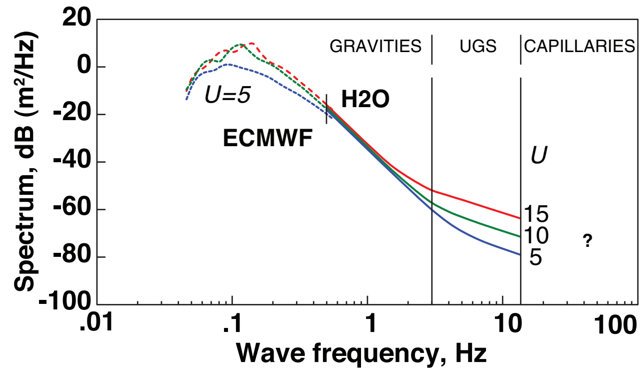

FIG. 4. The wave model based on H2O bottom data (solid lines) merges smoothly with ECMWF models of the wave field over H2O (dotted lines). The H2O spectra for 15 and 5 m s^{-1} have been displaced ±1 dB so they are distinguishable in the gravities. The ECMWF spectra are averages of spectra about the indicated wind from all year 2000 6-hourly models.

E. Gravity-ultragravity transition

The transition from long to short gravity waves has a long history. The generation of gravities is generally associated with wind shear at a critical layer where phase velocity c equals wind speed U;[12] the generation process of the unltragravities remains unknown!

Janssen[13] places the junction at a wave number $\kappa_{join} = g/u_\star^2$ where the phase velocity is the friction velocity; for a $6\,\mathrm{m\,s^{-1}}$ wind we have $u_\star = 0.21\,\mathrm{m\,s^{-1}}$ and $\kappa_{join}(6) = 213\,\mathrm{radians\,m^{-1}}$ (wave length 3 cm). We proceed by equating the two terms in (1), using the parameters in (7),

$$\kappa_{join}(U) = 168\ \exp(-.15U) \tag{8}$$

This yields a much lower wave number, $\kappa_{join}(6) = 68\,\mathrm{radians\,m^{-1}}$, for a wavelength of 10 cm.

F. Mean-square slope

Fig. 5A shows the contributions to the mean-square slope for the two wave bands, with

$$\langle m_G^2(U)\rangle = \int_{\kappa_p}^{\kappa_{join}} \kappa^2 F_\zeta(\kappa, U)\kappa d\kappa \tag{9a}$$

$$\langle m_{UG}^2(U)\rangle = \int_{\kappa_{join}}^{\kappa_{min}} \kappa^2 F_\zeta(\kappa, U)\kappa d\kappa \tag{9b}$$

The lower limit of the gravities is taken at $\kappa_p = g/U^2$, where $c_p = U$, κ_{join} is given by (8), and κ_{min}, the wave number of the phase velocity minimum, defines the boundary between ultragravity and capillary waves. The conclusions are that: (i) up to $U = 5\ \mathrm{m\,s^{-1}}$ the H2O-derived mean-square slopes are in general agreement with the glitter derived slopes because in the gravities the inferred wave spectrum is close to the Phillips spectrum, but (ii) for higher winds the H2O-derived values are several times higher. There is no easy way to reconcile the

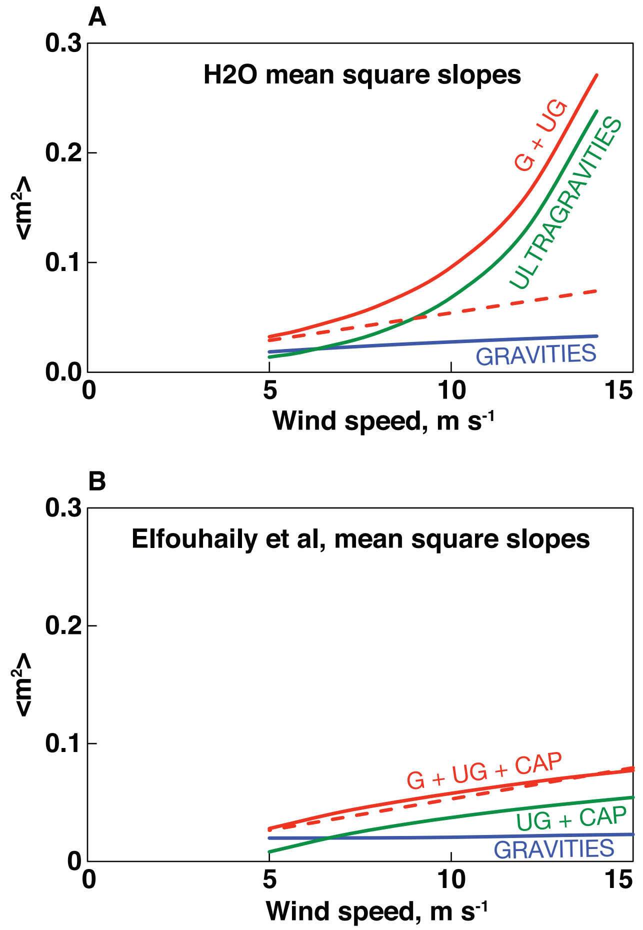

FIG. 5. (A) H2O mean square slope components. The dashed red line is the sum of up-wind and down-wind glitter slopes plotted in Fig 7. (B) Mean square slopes for the Elfouhaily *et al.* wave model. Adapted from their Fig 7.

H2O exponential wind dependence with the glitter linear dependence. We return to this enigma in Section VIII.

IV. EVIDENCE FROM (NEAR) THE SEA SURFACE

Observational evidence on the elevation spectrum of wind waves available by 1997 was summarized by Elfouhaily *et al.*[14] in an important paper, *The unified directional spectrum for long and short wind-driven waves*, that has been the foundation of many subsequent analyses of microwave emission and backscatter (e.g. Refs. 15, 16). The model (henceforth, E model) spans wave numbers from the low-frequency wind peak to 1,000 radians m^{-1}, thus including the gravities and ultragravities, and extending well into the capillaries. The E model was tailored in the ultragravity and capillary bands to be consistent with the Cox & Munk linear dependence of mean-square slope on wind speed (Fig 5B).

Shortly afterwards, Janssen *et al.*[13] derived a similar model (V model), featuring a Phillips-like spectrum in the gravities, joined to an ultragravity spectrum computed from the energy balance principle. The V model is also consistent with the Cox & Munk relationship.

Subsequent studies of the ultragravities (*e.g.* microwave radiometry, laser slope measurements, energy balance modeling, and interpretations of geophysical model functions, Refs. 17–21) have been in overall agreement with the E and V models. A $\kappa^{-3.5}$ power law is representative of the wave number dependence of $F_\zeta(\kappa, U)$ in the ultragravity band, only slightly flatter than the classical κ^{-4} Phillips spectrum in the gravity band. Further, in most models the change in the ultragravity elevation spectrum with U lessens with increasing wind (unlike the exponential H2O dependence).

A comparison of the H2O velocity spectra observed on the sea floor with those inferred from the E model reveals sharp differences in the ultragravities (Fig. 6A): (i) a rise (as compared to a fall) in spectral intensity with frequency, and (ii) a constant gradient (as compared to a decreasing gradient) of intensity (in dB's) with increasing wind speed. The difference between the observed acoustics and the acoustics of the E model is plotted in Fig. 6B. As expected, the difference spectrum is associated with an exponential wind dependence of approximately $3\,\mathrm{dB}/(\mathrm{m\,s}^{-1})$.

V. EVIDENCE FROM ABOVE THE SEA SURFACE

Fig. 7 gives the result of satellite glitter measurements: mean-square slopes in the up-down and cross wind directions. Slope statistics is based on almost ten million reflectance measurements distributed globally,[22] and so the error bars (circle diameters) are very tight; the red lines are based on 29 images taken from B17 aircraft fifty years ago,[23] but comments concerning the reflection of sunlight from the sea surface go back to antiquity.[24]

Observations in Fig. 7 yield the following empirical relations:

1. The ratio crosswind/downwind of mean-square slope components equals approximately $\langle m_y^2\rangle/\langle m_x^2\rangle = 2/3$ for a range of wind speeds.

2. Total mean-square slope varies linearly with wind according to $\langle m^2\rangle = (4 + 5U) \times 10^{-3}$ (wind in $\mathrm{m\,s}^{-1}$).

The glitter slope variance is in quantitative agreement with the H2O slopes at a wind speed of 5 $\mathrm{m\,s}^{-1}$, the lowest for which there are reliable ultragravity data (Fig. 5A). Up to this speed the slope is dominated by the gravities. At high winds the ultragravities dominate, and the bottom-derived slopes rise sharply above the glitter slopes.

Unlike the optical measurements, space observations with microwave frequency probes are of limited usefulness for independent assessment of ocean wave properties. It is not yet possible to measure the spectrum of the ultragravities directly.[25] Radar observations, however, can give the slope at a limited number of discrete wave numbers, depending on the frequency and inclination angle.[7]

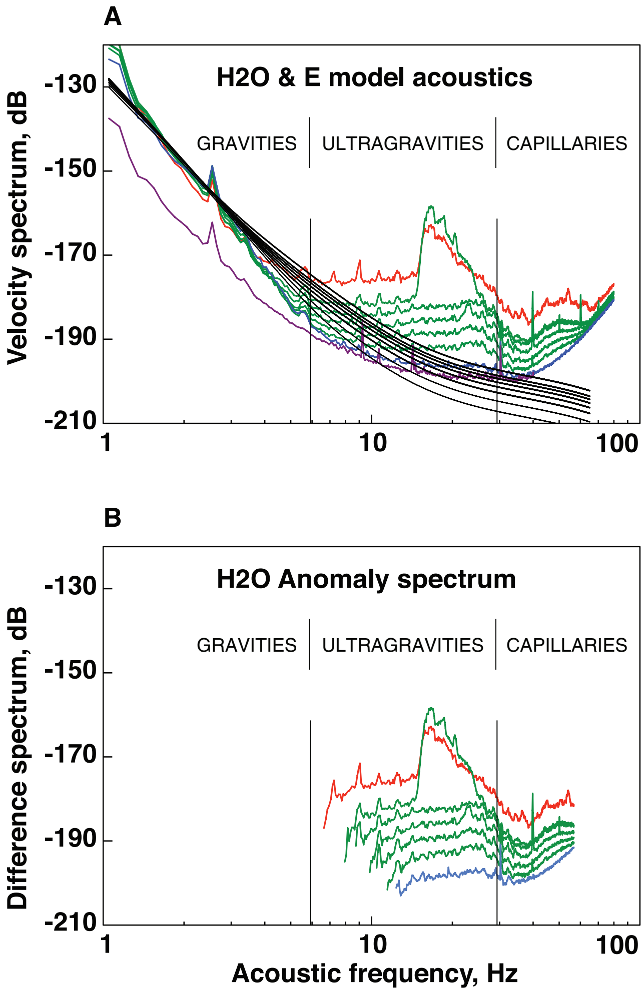

FIG. 6. (A) The spectrum of acoustic radiation of the Elfouhaily wave model (black) is appreciably less than the observed H2O velocity spectrum (colored) in the ultragravities. Wind speeds for the five green spectra are equally spaced from 8 to 12 $\mathrm{m\,s^{-1}}$. The red (blue) are for 14 (6) $\mathrm{m\,s^{-1}}$. The speeds are determined by the power at 11.5 Hz for each spectrum. The same speeds are used for the spectra of the E model. (B) The anomaly spectrum is the difference, in the ultragravity band, between the H2O spectrum and the vertical velocity derived from the E model.

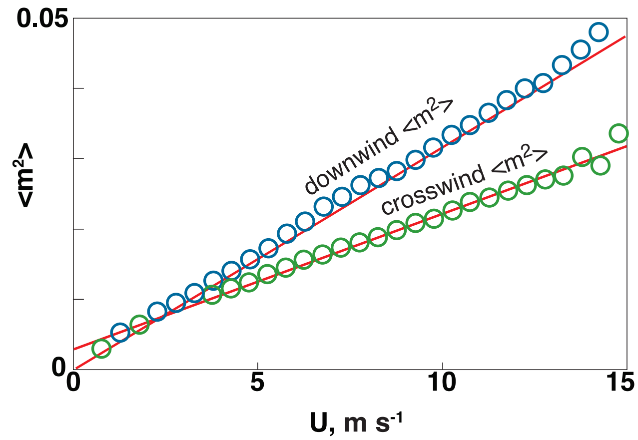

FIG. 7. Mean square slopes derived from glitter measurements taken from satellites (circles) and aircraft (lines).

VI. A HYBRID MODEL

There are a number of ways to interpret the discrepancy between the mean-square slopes measured from above as compared to those inferred from the H2O bottom measurements. Here we consider a hybrid model in which the total bottom acoustics (TBA) consists of the pressure and velocity bottom signatures inferred from the E model (EBA, Elfouhaily bottom acoustics) plus acoustic signatures from an unknown source, call them bubble bottom acoustics (BBA).

The distance between the paired colored and black dB levels in Fig. 6 are a measure of the ratio of the spectral intensities, TBA/EBA. This ratio increases quasi-linearly with the logarithm of frequency from 6-10 Hz upward. For high winds and frequencies, EBA is negligible, and BBA is nearly constant with frequency. Recall the high correlation of the TBA with wind speed (Fig. 2); a possible interpretation is that BBA is a manifestation of breakers and other sporadic wind generators of sound but not an inherent component of surface wave signatures. From the point of view of ambient sound in the abyssal ocean, the distinction between EBA and BBA is not vital.

Accordingly, the hybrid model consists of the EBA term (black curves in Fig. 6) plus the BBA term which is nearly independent of frequency. The BBA wind dependence can be fit by

$$\mathrm{BBA}: \; F_p(\omega_A) = 1.25 \times 10^{-13} U^6$$

or, alternatively,

$$\mathrm{BBA}: \; F_p(\omega_A) = 2.3 \times 10^{10} \exp(.62U)$$

Spectra for the hybrid model are shown by the black curves in Fig. 8. They are generally within 2 dB of the measured velocity spectra (colored curves, identical with Fig. 1) in the ultragravities. The hybrid model cannot account for the measured intensity drop near 30 Hz where the BBA term dominates. We have previously attributed this feature to a minimum in phase velocity or other wave singularities at half this frequency.

VII. DISCUSSION

Our interpretation of the H2O measurements is severely hindered by the lack of good surface records in the the ultragravity band of ocean waves. There is no theory of how they are generated. We lack good information about their directional distribution, a crucial element in coupling surface waves to sound waves. And finally, we have not allowed for interaction with the sea bottom. Other than that, the continuous three year H2O record, with the benefit of its mid-ocean location removed from human tampering, has been a surprisingly rich source of information.

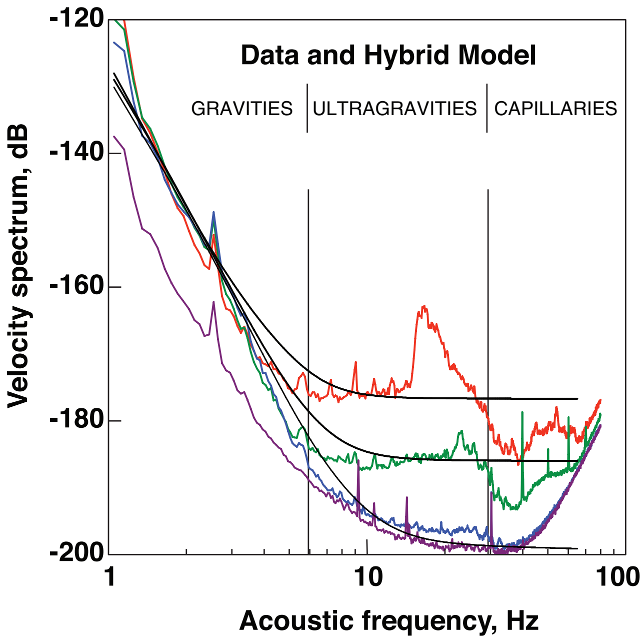

FIG. 8. Vertical velocity spectra used in Fig. 1 (colored) along with acoustic spectra for the hybrid model (black).

There is an opportunity for monitoring a variety of processes with low-noise bottom instruments. Satellite oceanography has demonstrated that an intensive sampling strategy can overcome some of the problems of remote sensing from above. It would appear that remote sensing from beneath could offer similar opportunities.

Regardless of our ignorance of the underlying physics, the lowest observed spectra (purple lines in Fig. 1) are remarkable, yet not without precedent. At 10 Hz under the lightest winds the H2O pressure spectrum (< -80 dB) is about the same as observations under similar conditions at ALOHA (Ref. 2, Figs. 3 and 6). This number is 20 dB below the Wenz model[26] at this frequency. Somewhat higher levels were seen on hydrophones near Wake Island.[4,27]

A bottom seismometer off California recorded levels down to -180 dB at 10 Hz when the wind was below $2\,\mathrm{m\,s^{-1}}$ (Ref. 29, Fig. 2, day 128, but the mislabled vertical axes ought to read acceleration with units $(\mu\mathrm{m\,s^{-2}})^2/\mathrm{Hz}$). This is considerably higher than the lowest H2O velocity spectrum (-197 dB), but with an ocean depth of only 3800 m, the bottom was not out of the sound channel. The H2O velocity spectrum at 10 Hz is consistent with the pressure spectrum, assuming the impedance measured at lower frequencies holds here. Unpublished spectra for hydrophones and seismometers from stations of the PLUME array[28] are similar to those from H2O data.

The model devised here, (1, 7), is generally consistent with the model developed to fit data from the hydrophone at ALOHA.[2] The affinities are easily shown by combining Dunnebier *et al.* Eqns. (5) and (6). Their initial model presumed a Phillips-like κ^{-4} wave spectrum in the gravities, but a closer fit to the acoustic observations was obtained when an *ad hoc* f_p^{-1} was appended to the Hughes equation (Ref. 2, Eqn. 5). Rolling this term into F_ζ yields at an additional factor $1.002\kappa^{-.25}$ for the gravities term of (Ref. 2, Eqn. 6). In addition, taking $U/u_\star = 25$, the coefficient for the exponential in the ultragravities wind term becomes 0.28. With these two transformations, and neglecting the exponential roll-offs at both ends of the wave spectrum, we get the following parameters for their model cast into our notation:

$$m = -4.25, \quad \beta = 0.024, \tag{10a}$$
$$n = -1.58, \quad \gamma = 5.0 \times 10^{-6}, \quad a = .28 \tag{10b}$$

There is better overall concordance in the gravities than the ultragravities, but it is very significant that both ultragravity models have an spectrum depending exponentially on wind, and with similar coefficients.

VIII. ENIGMA

We are left with an enigma. If we interpret the ultragravity band as the result of acoustic radiation by the Longuet-Higgins mechanism using conventional assumptions, then we are left with mean square slopes far above those indicated by the glitter observations. The hybrid model interprets the ultragravities as being the result of two processes: (i) acoustic radiation from Elfouhaily-like surface waves, plus (ii) acoustic radiation from an entirely different process, such as collapsing bubbles from breaking waves.

The data in the capillary band present similar problems. We are intrigued by the inflection near 30 Hz in the bottom spectra, and it is tempting to associate this inflection with the gravity-to-capillary transition in the wave field at half this frequency. This hypothesis is lost if the energy is not generated by a Longuet-Higgins mechanism.

The strong correlation of the ultragravity and capillary spectra with overhead winds shows that, whatever the generation mechanism, the winds drive it.

Acknowledgments

We acknowledge the extraordinary accomplishment of F. Duennebier and the entire H2O team for installation and operation of the H2O system, and thank the Iris Data Management Center for data curation. We are grateful to Xavier Zabalgogeazcoa at SAIC (now with Heat, Light, and Sound, Inc) and Jean Bidlot at the European Center for Medium-Range Weather Forecasts. The former helped in many ways, not least by calculating, numerous times, spectra for three years of data. The latter extracted several custom data sets from the ECMWF data base. W. E. Farrell is grateful for the support of Science Applications International Corporation during the early months of this research. W. Munk has the Secretary of the Navy Chair in Oceanography.

APPENDIX: ALIGNMENT OF THEORIES FOR THE ACOUSTIC WAVES RADIATED BY OCEAN GRAVITY-CAPILLARY WAVES

In the following discussion we summarize the extensive background to the acoustic radiation formula (Eq. 4) used in the text. This formula is based on the wave-wave interaction theory of Longuet-Higgins and Hasselmann, conventional assumptions for the dispersion relation, and generalizations by Brekhovskikh and others to allow for surface tension. Various small errors in the literature are rectified. Equations presented in the first two parts are give without citation.

1. Basic relations

Let $F_p(\omega_A)$ designate the spectrum of acoustic pressure radiated by the interaction of nearly oppositely directed surface waves with elevation spectrum $F_\zeta(\omega_S)$. The acoustic radiation is at twice the frequency of the surface waves. The power spectra are defined by the mean-squares

$$\begin{aligned}\langle p^2\rangle &= \int_0^\infty F_p(\omega_A)d\omega_A \\ \langle \zeta^2\rangle &= \int_0^\infty F_\zeta(\omega_S)d\omega_S \\ \omega_A &= 2\omega_S\end{aligned}$$

and, as shown below, are related according to

$$F_p\left(\omega_A\right) = \left[\frac{\pi}{8}\left(\frac{\rho}{c}\right)^2 \omega_A^6 \frac{v(\kappa_S)}{\kappa_S}\right] F_\zeta^2(\omega_S) R_B^2 I_\kappa \qquad \text{(A.1)}$$

In this equation, ρ and c are the density and sound velocity of sea water, and κ_S and $v(\kappa_S)$ are the wave number and group velocity of the surface waves. The term R_B is the "Brehovskikh ratio," and I_κ is the overlap integral, both defined below.

We use the deep water dispersion relation, expressed in terms of the wave number of the minimum phase speed κ_{min}, which depends on the surface tension $T = .074$ N m^{-1}.

$$\omega_S^2 = g\kappa_S\left(1+r^2\right), \; r = \kappa_S/\kappa_{min} \qquad \text{(A.2a)}$$

$$\kappa_{min} = \sqrt{\rho g/T} \; \approx 363 \text{ radians m}^{-1} \qquad \text{(A.2b)}$$

We also have the phase and group velocities

$$c = \omega_S/\kappa_S, \;\; c_{grav}^2 = g/\kappa, \;\; c_{cap}^2 = T\kappa/\rho \qquad \text{(A.3a)}$$

$$v = d\omega_S/d\kappa_S = c\left(\frac{1+3r^2}{2(1+r^2)}\right) \qquad \text{(A.3b)}$$

$$v_{grav} = \frac{1}{2}c_{grav}, \;\; v_{cap} = \frac{3}{2}c_{cap} \qquad \text{(A.3c)}$$

The symbol c in these expressions is not to be mistaken for the speed of sound in sea water, which is the meaning in (A.1) and everywhere else.

The Brekhovskikh ratio is

$$R_B = \frac{1+\frac{5}{4}r^2}{1+r^2}, \;\; R_{grav}^2 = 1, \;\; R_{cap}^2 = 1.5625 \qquad \text{(A.4)}$$

This term is only found in the Brekhovskikh derivation.

It is readily shown that for gravity waves, ($r \to 0$), equation (A.1) reduces to

$$F_p(\omega_A) = \frac{\pi}{2}\left(\frac{\rho g}{c}\right)^2 \omega_A^3 F_\zeta^2\left(\omega_S\right) I_\kappa \qquad \text{(A.5)}$$

Much of the literature is confined to gravity waves.

2. Wave definitions

It remains to specify the "overlap integral," I. We require to define the surface wave spectrum in $\kappa, \theta-$space

$$\langle \zeta^2\rangle = \int_0^\infty d\kappa \int_0^{2\pi} F_\zeta(\kappa,\theta)\kappa d\theta \qquad \text{(A.6)}$$

Let $H_\kappa(\theta)$ designate the directional distribution so normalized that $\int_0^{2\pi} H_\kappa(\theta)d\theta = 1$ at any desired scalar wave number κ. Thus, $F_\zeta(\kappa,\theta) = \bar{F}_\zeta(\kappa)H_\kappa(\theta)$, where $\bar{F}_\zeta(\kappa)$ is the spectral density at κ integrated over all directions. Omitting now the overbar, we then have

$$\langle \zeta^2\rangle = \int_0^\infty F_\zeta(\kappa)\kappa d\kappa = \int_0^\infty F_\zeta(\omega)d\omega \qquad \text{(A.7)}$$

With H_κ, the overlap integral is given as

$$I_\kappa = \int_0^{2\pi} H_\kappa(\theta)H_\kappa(\theta+\pi)d\theta \qquad \text{(A.8)}$$

In the frequency domain, H_ω, I_ω are similarly defined. For an isotropic wave field, $H = I = (2\pi)^{-1}$.

It follows from (A.7) that

$$F_\zeta(\omega) = F_\zeta(\kappa)\kappa\frac{d\kappa}{d\omega} = F_\zeta(\kappa)\frac{\kappa}{v} \qquad \text{(A.9)}$$

and as a consequence

$$\frac{v}{\kappa}F_\zeta^2(\omega) = \frac{\kappa}{v}F_\zeta^2(\kappa) \qquad \text{(A.10)}$$

Substituting (A.10) in (A.1) gives the alternate expression

$$F_p\left(\omega_A\right) = \left[\frac{\pi}{8}\left(\frac{\rho}{c}\right)^2 \omega_A^6 \frac{\kappa_S}{v(\kappa_S)}\right] F_\zeta^2(\kappa_S) R_B^2 I_\kappa \qquad \text{(A.11)}$$

3. Longuet-Higgins (1950) and Hasselmann (1963)

The beginning was Longuet-Higgins' landmark paper[30] which quantitatively demonstrated that microseisms, the world-wide seismic noise background, with spectrum peaking around $f = 1/6$ Hz, were due to the interaction of opposed ocean waves. The same methodology has recently been applied to model microseisms in North America as arising from waves in the North Atlantic.[31] The connection between Longuet-Higgins' approach and Hasselmann's has been elucidated by Ardhuin *et al.* (Ref. 32, Appendix A).

In a broad-ranging paper,[33] Hasselmann considered three mechanisms of microseism generation, and concluded that the cause was non-linear wave-wave interactions, as Longuet-Higgins had proposed over a decade before.

To obtain the familiar result we start with Hasselmann's (2.15), correcting the misprint and adding subscripts to distinguish between wave and acoustic variables.

$$F_p\left(\kappa_A,\omega_A\right)=\omega_A\frac{(\rho g)^2}{2}\int_0^{2\pi} f_\zeta\left(\omega_S,\theta\right) f_\zeta\left(\omega_S,\theta+\pi\right) d\theta \tag{A.12}$$

Factoring the wave spectrum into a magnitude part and a directional part, as before, gives

$$F_p\left(\kappa_A,\omega_A\right)=\omega_A\frac{(\rho g)^2}{2}F_\zeta^2\left(\omega_S\right)\int_0^{2\pi} H\left(\theta\right) H\left(\theta+\pi\right) d\theta \tag{A.13}$$

It is noteworthy that the pressure spectrum is independent of the vector wave number of the acoustic field. The total pressure at a point is the integral over all (acoustic) wave numbers. But the acoustic wave number cannot exceed ω_A/c. Using $\vec{\kappa}$ for the vector wave number, we have

$$\begin{aligned}F_p\left(\omega_A\right)&=\int_{-\infty}^{\infty} F_p\left(\vec{\kappa},\omega_A\right) d\vec{\kappa}\\&=\int_0^{\omega_A/c}\int_0^{2\pi} F_p\left(\kappa,\omega_A\right)\kappa d\kappa d\phi\end{aligned} \tag{A.14}$$

Carrying out the two integrations, which yields the term in braces, gives

$$\begin{aligned}F_p\left(\omega_A\right)=\omega_A\frac{(\rho g)^2}{2}F_\zeta^2\left(\omega_S\right)&\int_0^{2\pi} H\left(\theta\right) H\left(\theta+\pi\right) d\theta\\\times\left\{\pi\left(\frac{\omega_A}{c}\right)^2\right\}&\end{aligned} \tag{A.15}$$

leading immediately to (A.5).

4. Subsequent literature

Brekhovskikh[34,35] was the first in the field to consider surface tension, but his formula must be doubled so that it reduces to (A.5) in the gravity wave limit. This was discovered by Hughes and reported by Lloyd.[36] His formula also incorporates the "Brekhovskikh ratio" which makes it 50% larger in the capillaries than the corrected results of Hughes and Cato.

We start with equation (13) in the second reference, mostly keeping the original notation, adding subscripts where needed, and adding the correction term in braces.

$$\begin{aligned}F_p\left(\omega_A\right)=\{2\}\,&\frac{\pi}{4}\left(\frac{\rho}{c}\right)^2\omega_S^2\left(5\omega_S^2-g\kappa_S\right)^2\\&\times\left[\left(\kappa\frac{\partial\kappa}{\partial\omega}\right)^{-1}\Phi^2(\omega_S)\right]\frac{\mathrm{m}}{\delta\psi}\end{aligned} \tag{A.16}$$

The two substitutions

$$F_\zeta^2\left(\omega_S\right)=\Phi^2(\omega_S),\quad I_\kappa=\frac{\mathrm{m}}{\delta\psi} \tag{A.17}$$

and introduction of the group velocity, v, give

$$F_p\left(\omega_A\right)=\frac{\pi}{2}\left(\frac{\rho}{c}\right)^2\omega_S^2\left(5\omega_S^2-g\kappa_S\right)^2\left[\frac{v(\kappa_S)}{\kappa_S}F_\zeta^2(\omega_S)\right]I_\kappa \tag{A.18}$$

Rearranging terms, switching to ω_A, and introducing R_B, as defined in (A.4), leads to the form

$$F_p\left(\omega_A\right)=\left[\frac{\pi}{8}\left(\frac{\rho}{c}\right)^2\omega_A^6\frac{v(\kappa_S)}{\kappa_S}\right]F_\zeta^2(\omega_S)R_B^2 I_\kappa \tag{A.19}$$

which is (A.1).

Hughes,[37] working in the wave number domain, derived a result (equation 33) twice as large as (A.11), as he himself realized and communicated to Lloyd.[36] Showing this correction in braces, his formula,

$$F_p\left(\omega_A\right)=\left\{\frac{1}{2}\right\}\left[\frac{\pi}{4}\left(\frac{\rho}{c}\right)^2\omega_A^6\frac{\kappa_S}{v(\kappa_S)}\right]F_\zeta^2(\kappa_S)I_\kappa \tag{A.20}$$

is (A.11), with $R_B=1$.

Lloyd[36] (unnumbered equation at the bottom of p. 433) published a formula equivalent to (A.5), which holds when surface tension is ignored. This is easily demonstrated by expressing all spectra in radian frequency, recognizing the different definition of the overlap integral, and accounting for the fact he specifically incorporated the Phillips model ($F_\zeta(\omega)=\beta g^2\omega^{-5}$) given a few paragraphs previously in the paper.

His derivation started with consideration not only of surface tension but also of traveling wave contributions to the radiated energy. Although the influence of these terms was dropped part way through the analysis, and it is not clear how to recover them, he corroborated Brekhovskikh, stating on p. 433 (using our notation)

$$\frac{F_p(\text{Brek})}{F_p(\text{Llo})}=\left[1+\frac{r^2}{4\left(1+r^2\right)}\right]^2 \tag{A.21}$$

From this, we infer that he obtained, but did not publish, a result equivalent to (A.1), but with $R_B=1$. Equation (A.21) is identical to (A.4), but to obtain this form we use the equivalence $T=\kappa_{min}^{-2}$, as follows from his unconventional definition of the dispersion relation in the text following (18).

Cato[38,39] applied a theory of Lighthill's for acoustic radiation from moving boundaries in a fluid. In the first paper he obtained an exact solution, without resorting to the usual perturbation expansion. His approach may have some affinities with Lloyd's work, which also was based upon a Lighthill theory. The second paper, in which he applied the general result to the specific case of radiation by nearly opposed gravity waves, is more pertinent.

In the case of standing waves on the surface of a bottomless ocean, Cato's solution for the spectrum of the far field pressure (equation 59 in the second paper), partially using his notation, is

$$P_D(\omega_A)=\frac{1}{16}\left(\frac{\rho g}{c}\right)^2\omega_A^3\Omega_\zeta^2\left(\omega_S\right)I_\kappa \tag{A.22}$$

This is 8π smaller than (A.5).

More interesting is to tap earlier into his derivation, and it is not difficult to derive the analog of (A.1), but with the same 8π discrepancy. Starting with equation 54 in the same paper, and changing notation slightly (but retaining his H, which is not a spreading function), we have

$$P_D(\omega_A) = 2\rho^2\omega_S^4 \left\{ \frac{v(\kappa_S)}{\kappa_S} F_\zeta^2(\omega_S) \right\} I \int HH^* \kappa d\kappa \tag{A.23}$$

In (A.23) we have taken $i = l = 3$ as in the original, since this is the principle term in the far field. Furthermore, $H = H_3 = 1/2$ far from the surface, so

$$\int HH^* \kappa d\kappa = \frac{1}{4}\left(\frac{\omega_A^2}{2c^2}\right) \tag{A.24}$$

giving

$$P_D(\omega_A) = \left(\frac{\rho}{c}\right)^2 \omega_S^4 \left(\frac{\omega_A^2}{4}\right) \left\{ \frac{v(\kappa_S)}{\kappa_S} F_\zeta^2(\omega_S) \right\} I_\kappa \tag{A.25}$$

which is the same as

$$P_D(\omega_A) = \left[\frac{1}{64}\left(\frac{\rho}{c}\right)^2 \omega_A^6 \frac{v(\kappa_S)}{\kappa_S}\right] F_\zeta^2(\omega_S) I_\kappa \tag{A.26}$$

and (A.26) is, now, 8π smaller than (A.1), with $R_B = 1$.

Kibblewhite made major contributions to the subject, culminating in the monograph coauthored with Wu.[40] This covers not only their own work, but includes a review and summary of the foundations underlying most other derivations. There is one theoretical curiosity to be mentioned. By using pressure rather than velocity potential as the field variable in the perturbation expansion, they obtain an answer 20% smaller than (A.5). Substituting equations 4.109 and 4.111 in 4.92, the result following this approach is

$$F_p(\omega_A) = \left[\frac{26}{32}\right] \frac{\pi}{2} \left(\frac{\rho g}{c}\right)^2 \omega_A^3 F_\zeta^2(\omega_S) I_\kappa \tag{A.27}$$

Wilson *et al.*[41] applied Cato's theory to relate low frequency wave and acoustic data acquired off the East coast of North America. The deep acoustic data were well explained by using the measured wave spectrum as the source term in Cato's theory. Their method accounted for a variable sound speed profile in the water, and a layered and elastic ocean bottom. Although their work focused on frequencies less than 1 Hz, the method is equally applicable to higher frequencies. The agreement between theory and data is curious, because their theory also contains Cato's 8π error.

The governing equation is (3) in their paper, except for the erroneous ρ^2, and for the far field we take $i = j = 3$, as described above. Dropping subscripts,

$$P_D(\omega_A) = \frac{2}{(2\pi)^2} \int \Phi HH^* d\vec{\kappa} \tag{A.28}$$

Referring back to Cato's (34, 39, 40, and 41) in the second paper, and with some obvious changes of variable, it can be shown that

$$\Phi = 2\pi\rho^2\omega_S^4 \frac{v(\kappa_S)}{\kappa_S} F_\zeta^2(\omega_S) \tag{A.29}$$

and thus can be brought outside the integral.

The integral that remains is 2π times (A.24), when the angular term is considered. This gives,

$$F_p(\omega_A) = \left[\frac{1}{64}\left(\frac{\rho}{c}\right)^2 \omega_A^6 \frac{v(\kappa_S)}{\kappa_S}\right] F_\zeta^2(\omega_S) I_\kappa \tag{A.30}$$

which is the same as (A.26) and 8π smaller than (A.1), with $R_B = 1$.

[1] F. K. Duennebier, D. W. Harris, J. Jolly, J. Babinee, D. Copson, and K. Stiffel, "The Hawaii-2 Observatory seismic system", IEEE J. Oceanic Eng. **17**, 212–217 (2002).

[2] F. K. Duennebier, R. Lukas, E. Nosal, J. Aucan, and R. Weller, "Wind, waves, and acoustic background levels at Station ALOHA", J. Geophys Res. **117**, 1–21 (2012).

[3] W. E. Farrell and W. Munk, "What do deep sea pressure fluctuations tell about short surface waves?", Geophys. Res. Let. **35**, 1–4 (2008).

[4] W. E. Farrell and W. Munk, "Booms and busts in the deep", J. Phys. Oceanogr. 2159–2169 (2010).

[5] W. J. Pierson and L. Moskowitz, "A proposed spectral form for fully developed wind sea based on the similarity theory of S. A. Kitaigorodskii", J. Geophys. Res. **69**, 5181–5190 (1964).

[6] J. H. G. M. Alves, M. L. Banner, and I. R. Young, "Revisiting the PiersonMoskowitz asymptotic limits for fully developed wind waves", J. Phys. Ocean. **33**, 1301–1323 (2003).

[7] P. A. Hwang, "A note on the ocean surface roughness spectrum", J. Atmos. Ocean. Tech.. **28**, 436–443 (2011).

[8] R. J. Urick, "Sea-bed motion as a source of ambient noise background of the sea", J. Acoust. Soc. Am. **56**, 1010–1011 (1974).

[9] S. C. Webb, "The equilibrium oceanic microseism spectrum", J. Acoust. Soc. Am. **92**, 2141–2158 (1992).

[10] W. Munk, P. Worcester, and C. Wunsch, *Ocean Acoustic Tomography* (Cambridge University Press, Cambridge) (1995), 216-217.

[11] P. A. E. M. Janssen, "Progress in ocean wave forecasting", J. Comp. Phys. **227**, 3572–3594 (2008).

[12] J. W. Miles, "On the generation of surface waves by shear flows", J. Fluid Mech. **3**, 185–204 (1957).

[13] P. A. E. M. Janssen, H. Wallbrink, C. J. Calkoen, D. van Halsema, W. A. Oost, and P. Snoeij, "Viers-1 scatterometer model", J. Geophys. Res. **103**, 7807–7831 (1998).

[14] T. Elfouhaily, B. Chapron, K. Katsaros, and D. Vandemark, "A unified directional spectrum for long and short wind-driven waves", J. Geophys. Res. **102**, 15,781–15,796 (1997).

[15] W. J. Plant, "A stochastic, multiscale model of microwave backscatter from the ocean", J. Geophys. Res. **107**, 1–21 (2002).

[16] P. A. Hwang and W. J. Plant, "An analysis of the effects of swell and surface roughness spectra on microwave backscatter from the ocean", J. Geophys. Res. **115**, 1–14 (2010).

[17] A. V. Kuzmin and M. N. Pospelov, "Retrieval of gravity-capillary spectrum parameters by means of microwave radiometric techniques", IEEE Trans. Geoscience and Remote Sens. **43**, 983–989 (2005).

[18] P. A. Hwang, "A study of the wavenumber spectra of short water waves in the ocean. Part II: spectral model and mean square slope", J. Atmos. and Ocean. Tech. **14**, 1174–1186 (1997).

[19] N. Pierdicca and L. Pulvirenti, "Comparing scatterometric and radiometric simulations with geophysical model functions to tune a sea wave spectrum model", IEEE Trans. Geoscience and Remote Sensing **46**, 3756–3767 (2008).
[20] V. N. Kudryavtsev, V. K. Makin, and B. Chapron, "Coupled sea surface-atmosphere model 2. Spectrum of short wind waves", J. Geophys. Res. **104**, 7625–7639 (1999).
[21] D. R. Lyzenga, "Ocean wave spectrum and dissipation rate derived from CMOD4 model function", J. Geophys. Res. **109**, 1–9 (2004).
[22] F. M. Bréon and N. Henriot, "Spaceborne observations of ocean glint reflectance and modeling of wave slope distributions", J. Geophys. Res **111, C06005**, 1–10 (2006).
[23] C. Cox and W. Munk, "Measurement of the roughness of the sea surface from photographs of the sun's glitter", J. Optical. Soc. Am. **44**, 838–850 (1954).
[24] G. Galilei, *Dialogue concerning the two chief world systems* (Modern Library, New York) (2001), trans. Stillman Drake, p. 112.
[25] I. S. Robinson, *Measuring the oceans from space* (Springer, Berlin) (2004), 669 p.
[26] G. M. Wenz, "Acoustic ambient noise in the ocean: spectra and sources", J. Acoust. Soc. Am. **34(12)**, 1936–1957 (1962).
[27] C. S. McCreery, F. K. Duennebier, and G. H. Sutton, "Correlation of deep ocean noise (0.4-30 hz) with wind, and the Holu spectrum - A worldwide constant", J. Acoust. Soc. Am. **93**, 2639–2648 (1993).
[28] G. Laske, J. A. Collins, C. J. Wolfe, S. C. Soloman, R. S. Detrick, J. A. Orcutt, D. Bercovici, and E. H. Hauri, "Probing the Hawaiian Hot Spot with new broadband ocean bottom instruments", EOS **90**, 362–363 (2009).
[29] L. M. Dorman, A. E. Schreiner, L. D. Bibee, and J. A. Hildebrand, "Deep-water sea-floor array observations of seismo-acoustic noise in the Eastern Pacific and comparison with wind and swell", in *Natural physical sources of underwater sound*, edited by B. R. Kerman, 165–174 (Kluwer Academic Publishers, Netherlands) (1993).
[30] M. S. Longuet-Higgins, "A theory of microseisms", Philos. Trans. Roy. Soc. London **243**, 1–35 (1950).
[31] S. Kedar, M. Longuet-Higgins, F. Webb, N. Graham, R. Clayton, and C. Jones, "The origin of deep ocean microseisms in the North Atlantic ocean", Proc. Roy. Soc. London **A464**, 777–793 (2008).
[32] F. Ardhuin, E. Stutzmann, M. Schimmel, and A. Mangeney, "Ocean wave sources of seismic noise", J. Geophys. Res, **111**, 1–21 (2011).
[33] K. Hasselmann, "A statistical analysis of the generation of microseisms", Rev. Geoph. **1**, 177–210 (1963).
[34] L. M. Brekhovskikh, "Underwater sound waves generated by surface waves in the ocean", Izv. Acad. Sci. USSR, Atmos. Oceanic Phys. **2**, 970–980 (1966).
[35] L. M. Brekhovskikh, "Generation of sound waves in a liquid by surface waves", Sov. Phys. Acoust. **12**, 323–350 (1967).
[36] S. P. Lloyd, "Underwater sound from surface waves according to the Lighthill-Ribner theory", J. Acoust. Soc. Am. **69**, 425–435 (1981).
[37] B. Hughes, "Estimates of underwater sound (and infrasound) produced by nonlinearly interacting ocean waves", J. Acoust. Soc. Am. **60**, 1032–1360 (1976).
[38] D. H. Cato, "Sound generation in the vicinity of the sea surface: Source mechanisms and the coupling to the received sound field", J. Acoust. Soc. Am **89**, 1076–1095 (1991).
[39] D. H. Cato, "Theoretical and measured underwater noise from surface wave orbital motion", J. Acoust. Soc. Am **89**, 1096–1112 (1991).
[40] A. C. Kibblewhite and C. Y. Wu, *Wave interactions as a seismo-acoustic source* (Springer, Berlin) (1996), 313 p.
[41] D. K. Wilson, G. V. Frisk, T. E. Lindstrom, and C. J. Sellers, "Measurement and prediction of ultralow frequency ocean ambient noise off the eastern U.S. coast", J. Acoust. Soc. Am. **113**, 3117–3133 (2003).